Inorg. Chem. **2005**, *44*, 8740–8748

Electroactive Ligands: The First Metal Complexes of Tetrathiafulvenyl–Acetylacetonate

Julien Massue,[†] Nathalie Bellec,[†] Stéphanie Chopin,[‡] Eric Levillain,*[,‡] Thierry Roisnel,[§] Rodolphe Clérac,[||] and Dominique Lorcy*[,†]

Groupe Hétérochimie et Matériaux Electroactifs, SESO UMR 6510 CNRS—Université de Rennes 1, Institut de Chimie de Rennes, Campus de Beaulieu, Bât 10A, 35042 Rennes Cedex, France, Groupe Systèmes Conjugués Linéaires, Chimie, Ingénierie Moléculaire et Matériaux d'Angers, UMR CNRS 6200 - Université d'Angers, 2 Bd Lavoisier, 49045 Angers, France, Laboratoire de Chimie du Solide et Inorganique Moléculaire, UMR 6511 CNRS—Université de Rennes 1, Institut de Chimie de Rennes, Campus de Beaulieu, Bât 10B, 35042 Rennes Cedex, France, and Centre de Recherche Paul Pascal, CNRS UPR-8641, 115 av. Albert Schweitzer, 33600 Pessac, France

Received June 22, 2005

The reaction of tris(alkylthio)tetrathiafulvalene thiolates with 3-chloro-2,4-pentanedione affords tetrathiafulvalene (TTF) moieties substituted by the acetylacetone function (TTFSacacH), precursors of novel redox-active ligands: the acetylacetonate ions (TTFSacac). These TTFSacacHs have been characterized by X-ray diffraction analyses, and similar trends have been observed, such as a TTF core almost planar and the acetylacetone substituent located in a plane almost perpendicular to the plane formed by the TTF core. Their chelating ability has been demonstrated by the formation of the corresponding $M(TTFSacac)_2(pyridine)_2$ complexes in the presence of $M^{II}(OAc)_2 \cdot H_2O$ ($M = Ni^{2+}$, Zn^{2+}). These complexes with TTFSacac moieties, $Ni(TTFSacac)_2(pyridine)_2$, **6b**, and $Zn(TTFSacac)_2(pyridine)_2$, **7b**, have been characterized by X-ray diffraction analyses, showing in all structures the metal(II) center chelated by two TTFacac units in the equatorial plane and the octahedral coordination geometry around the metal completed by two axial pyridine ligands. Cyclic voltammetry and UV–visible–near infrared spectroscopic measurements have evidenced a sizable interaction between the two electroactive ligands and the stabilization of a mixed-valence state in the one-electron oxidized complexes.

Introduction

Various redox-active ligands where the electroactive lead is played by the tetrathiafulvalene (TTF) moiety have been prepared with the aim of forming, via their coordination to a transition metal, novel hybrid organic–inorganic building blocks. Depending on the coordination function and on the number of free coordination sites, modulation of the molecular architectures and electronic properties can be envisioned in regard to the preparation of multifunctional materials.[1] For instance, a variety of hybrid molecules acting as monodentate or polydentate redox-active ligands has been built on the basis of TTFs functionalized by phosphine,[2−5] dithiolate,[6] and pyridine.[7−9] The acetylacetonate ion formed in a basic medium from the acetylacetone also presents powerful chelating properties and forms complexes with various transition metals and main group elements.[10] For that

* To whom correspondence should be addressed. E-mail: dominique.lorcy@univ-rennes1.fr (D.L.), eric.levillain@univ-angers.fr (E.L.). Fax: (+33)-2-23-23-67-38 (D.L.).

[†] Groupe Hétérochimie et Matériaux Electroactifs, CNRS—Université de Rennes 1.

[‡] Université d'Angers.

[§] Laboratoire de Chimie du Solide et Inorganique Moléculaire, CNRS—Université de Rennes 1.

[||] Centre de Recherche Paul Pascal.

(1) (a) Coronado, E.; Day, P. *Chem. Rev.* **2004**, *104*, 5419. (b) Coronado, E.; Galán-Mascarós, J. R.; Gómes-Garcia, C. J.; Laukhin, V. *Nature* **2000**, *408*, 447.

(2) (a) Fourmigué, M.; Batail, P. *Bull. Soc. Chim. Fr.* **1992**, *129*, 29. (b) Fourmigué, M.; Uzelmeier, C. E.; Boubekeur, K.; Bartley, S. L.; Dunbar, K. R. *J. Organomet. Chem.* **1997**, *529*, 343. (c) Uzelmeier, C. E.; Bartley, S. L.; Fourmigué, M.; Rogers, R.; Grandinetti, G.; Dunbar, K. R. *Inorg. Chem.* **1998**, *37*, 6706. (d) Avarvari, N.; Martin, D.; Fourmigué, M. *J. Organomet. Chem.* **2002**, *643−644*, 292. (e) Devic, T.; Batail, P.; Fourmigué, M.; Avarvari, N. *Inorg. Chem.* **2004**, *43*, 3136. (f) Avarvari, N.; Fourmigué, M. *Chem. Commun.* **2004**, 1300.

(3) Smucker, B. W.; Dunbar, K. R. *J. Chem. Soc., Dalton Trans.* **2000**, 1309.

(4) Cerrada, E.; Diaz, C.; Diaz, M. C.; Hursthouse, M. B.; Laguna, M.; Light, M. E. *J. Chem. Soc., Dalton Trans.* **2002**, 1104.

(5) Pellon, P.; Gachot, G.; Le Bris, J.; Marchin, S.; Carlier, R.; Lorcy, D. *Inorg. Chem.* **2003**, *42*, 2056.

10.1021/ic051017r CCC: $30.25
Published on Web 10/20/2005

purpose, we previously presented the synthesis of trimethyl TTF substituted by acetylacetone groups $Me_3TTF(SacacH)$, **1**, and $Me_2TTF(SacacH)_2$, **2**, as potential electroactive ligands.[11] In the course of our investigations on the coordinating ability of **1** toward various metal cations ($M = Cu^{2+}$, Ni^{2+}, Co^{2+}, and Mn^{2+}), we observed the formation of the expected complexes that were completely insoluble in the usual organic solvents. Actually, this insolubility precluded any further characterization such as electrochemical investigations or the use of these building blocks to prepare materials. Therefore, this inconvenience drew us back to the synthesis of some more soluble ligands.

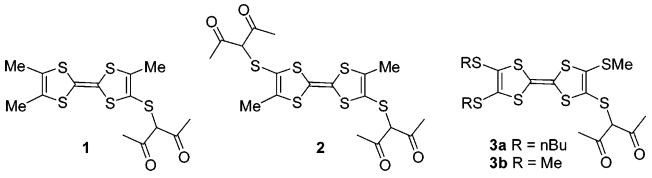

Taking advantage of the ability of the alkylthio substituents to increase the solubility of the TTF derivatives, we oriented our research on the synthesis of tris(alkylthio) (R = Me, Bu) TTF substituted by only one acetylacetone group, tris(alkylthio)TTF(SacacH), **3**. Herein, we report the synthesis and the chelating ability of these novel redox-active ligands toward metal(II) centers (M = Ni, Zn). The structural and electrochemical properties of the very first complexes with TTF(Sacac) moieties obtained with Ni and Zn are, thus, presented showing a sizable interaction between the TTF cores through the $M(acac)_2$ bridge.

Experimental Section

All reagents are commercially available and were used without further purification. Bis(butylthio)-bis(cyanoethylthio) TTF, **4a**;[12] bis(methylthio)-bis(cyanoethylthio) TTF, **4b**;[12] and tri(methylthio)-cyanoethylthio TTF, **5b**,[13] were synthesized according to literature procedures. Melting points were measured on a Kofler hot-stage apparatus and are uncorrected. ^{1}H NMR and ^{13}C NMR spectra were recorded on a Bruker ARX 200 spectrometer. Chemical shifts are quoted in parts per million (ppm) and referenced to tetramethylsilane. Mass spectra were recorded with a Varian MAT 311 instrument by the Centre Régional de Mesures Physiques de l'Ouest, Rennes. Elemental analyses were performed at the Laboratoire Central de Microanalyse du CNRS, Lyon. Chromatography was performed using silica gel, Merck 60 (70−260 mesh). Cyclic voltammetry has been performed in a three-electrode cell equipped with a platinum millielectrode and a platinum wire counter electrode. A silver wire served as a quasi-reference electrode, and its potential has been checked against the ferrocene/ferricinium couple (Fc^+/Fc) before and after each experiment. The electrolytic media involved CH_2Cl_2 and 0.2 mol L^{-1} tetrabutylammonium-hexafluorophosphate (TBAHP). All experiments were performed in a glovebox containing dry, oxygen-free (<1 ppm) argon at room temperature (RT). Electrochemical experiments have been carried out with an EGG PAR 273A potentiostat with positive feedback compensation. On the basis of repetitive measurements, absolute errors on potentials have been found to be around ±5 mV. The number of electrons was determined under thin-layer conditions. The deconvoluted voltammograms were calculated with Condecon software. The spectroelectrochemical setup[14] was realized in 0.2 M TBAHP/CH_2Cl_2. A Lambda 19 near infrared (NIR) Perkin-Elmer spectrophotometer was employed to record the optical spectra.

3-{[4′,5′-Bis(butylthio)-5-(methylthio)-2,2′-bi-1,3-dithol-4-yl]-thio}propane Nitrile, 5a. To a solution of bis(butylthio)-bis-(cyanoethylthio) TTF, **4a** (850 mg, 1.55 mmol), in 15 mL of *N*,*N*-dimethylformamide (DMF) was slowly added, under argon, a solution of $CsOH·H_2O$ (260 mg, 1.55 mmol) in 3 mL of MeOH. The mixture was allowed to stir for 30 min at RT, after which iodomethane (0.15 mL, 2.4 mmol) was added. Stirring was continued for 1 h. Solvents were rotary evaporated, and the resulting oil was extracted with CH_2Cl_2 and washed with water. The organic extract was purified by column chromatography over silica with CH_2Cl_2/PE (2:1) as the eluent to afford TTF **5** (760 mg, 96%) as an orange powder; mp 92−93 °C and $R_f = 0.49$. ^{1}H NMR ($CDCl_3$, δ): 0.94 (t, 6H), 1.36−1.68 (m, 8H), 2.51 (s, 3H), 2.73 (t, 2H), 2.85 (t, 4H), 3.05 (t, 2H). ^{13}C NMR (DMSO-d_6 + $CDCl_3$, δ): 13.8, 18.7, 21.4, 31.3, 31.6, 35.6, 108.6, 111.2, 118.7, 127.5, 128.0. HRMS: calcd for $C_{18}H_{25}NS_8$, 510.9753; found, 510.9750. Anal. Calcd for $C_{18}H_{25}NS_8$: C, 42.24; H, 4.92; S, 50.11. Found: C, 42.56; H, 4.86; S, 50.44.

3-{[4′,5′-Bis(butylthio)-5-(methylthio)-2,2′-bi-1,3-dithol-4-yl]-thio}pentane-2,4-dione, 3a. To a solution of tris(methylthio)-cyanoethylthio TTF, **5b** (760 mg, 1.49 mmol), in 15 mL of DMF was slowly added, under argon, a solution of $CsOH·H_2O$ (290 mg, 1.75 mmol) in 3 mL of MeOH. The mixture was allowed to stir for 30 min at RT, after which 3-chloro-2,4-pentandione (0.2 mL, 1.75 mmol) was added. Stirring was continued for 1 h. Solvents were rotary evaporated, and the resulting oil was extracted with CH_2Cl_2 and washed with water. The organic extract was purified by column chromatography over silica with CH_2Cl_2/PE (2:1) as the eluent to afford TTF **3a** (630 mg, 79%) as a red powder; mp 84−86 °C and $R_f = 0.72$. ^{1}H NMR ($CDCl_3$, δ): 0.96 (t, 6H), 1.38−1.55 (m, 4H), 1.56−1.72 (m, 4H), 2.45 (s, 3H), 2.50 (s, 6H), 2.85 (t, 4H), 17.23 (s, 1H). ^{13}C NMR (DMSO-d_6 + $CDCl_3$, δ): 13.7, 19.1, 21.3, 24.9, 31.6, 35.6, 102.8, 108.9, 110.5, 120.3, 127.6, 197.6. IR (KBr, cm^{-1}): 1678 (C=O). HRMS: calcd for $C_{20}H_{28}O_2S_8$, 555.9855; found, 555.9849. Anal. Calcd for $C_{20}H_{28}O_2S_8$: C, 43.13; H, 5.07. Found: C, 43.57; H, 5.12.

3-{[4′,5,5′-Tris(methylthio)-2,2′-bi-1,3-dithol-4-yl]thio}pentane-2,4-dione, 3b. To a solution of tris(methylthio)-cyanoethylthio TTF, **5b** (640 mg, 1.5 mmol), in 15 mL of DMF was slowly added, under argon, a solution of $CsOH·H_2O$ (290 mg, 1.75 mmol) in 3 mL of MeOH. The mixture was allowed to stir for 30 min at RT, after which 3-chloro-2,4-pentadione (0.2 mL, 1.75 mmol) was added. Stirring was continued for 1 h. Solvents were rotary evaporated,

(6) Kobayashi, A.; Fujiwara, E.; Kobayashi, H. *Chem. Rev.* **2004**, *104*, 5243 (and references therein).
(7) (a) Iwahori, F.; Golhen, S.; Ouahab, L.; Carlier, R.; Sutter, J.-P. *Inorg. Chem.* **2001**, *40*, 6541. (b) Ouahab, L.; Iwahori, S.; Golhen, S.; Carlier, R.; Sutter, J.-P. *Synth. Met.* **2003**, *133−134*, 505. (c) Setifi, F.; Ouahab, L.; Golhen, S.; Yoshida, Y.; Saito, G. *Inorg. Chem.* **2003**, *42*, 1791.
(8) Liu, S.-X.; Dolder, S.; Franz, P.; Neels, A.; Stoeckli-Evans, H.; Decurtins, S. *Inorg. Chem.* **2003**, *42*, 4801.
(9) Devic, T.; Avarvari, N.; Batail, P. *Chem.−Eur. J.* **2004**, *10*, 3697.
(10) Siedle, A. R. Diketone and Related Ligands. In *Comprehensive Coordination Chemistry*; Wilkinson, G., Gillard, R. D., McCleverty, J. A., Eds.; Pergamon Press: Oxford, 1987; Vol. 2, pp 365−412.
(11) Bellec, N.; Lorcy, D. *Tetrahedron Lett.* **2001**, *42*, 3189.
(12) Le Narvor, N.; Robertson, N.; Wallace, E.; Kilburn, J. D.; Underhill, A. E.; Bartlett, P. N.; Webster, M. *J. Chem. Soc., Dalton Trans.* **1996**, 823.
(13) Simonsen, K. B.; Sventrup, N.; Lau, J.;. Simonsen, O.; Mork, P.; Kristensen, G. J.; Becher, J. *Synthesis* **1996**, 407.
(14) Gaillard, F.; Levillain, E. *J. Electroanal. Chem.* **1995**, *398*, 77.

Table 1. Crystal Data and Structure Refinement Parameters for **3a**, **3b**, **6bA**, **6bB**, and **7b**

structure parameter	3a	3b	6bA	6bB	7b
empirical formula	$C_{20}H_{28}O_2S_8$	$C_{14}H_{16}O_2S_8$	$C_{38}H_{40}N_2NiO_4S_{16}$	$C_{38}H_{40}N_2NiO_4S_{16}$	$C_{38}H_{40}ZnN_2O_4S_{16}$
molecular weight	556.90	472.75	1160.39	1160.39	1167.05
color	red	orange	orange	orange	orange
cryst system	monoclinic	monoclinic	monoclinic	monoclinic	monoclinic
space group	*Pn*	$P2_1/c$	$P2_1/a$	$C2/c$	$C2/c$
a (Å)	9.189(5)	8.2973(2)	9.883(5)	19.953(5)	19.928(5)
b (Å)	5.402(5)	15.7634(4)	23.837(5)	9.397(5)	9.342(5)
c (Å)	26.794(5)	15.8702(4)	12.395(5)	28.325(5)	28.076(5)
α (deg)	90	90	90	90	90
β (deg)	95.307(5)	102.580(1)	94.220(5)	107.370(5)	107.707(5)
γ (deg)	90	90	90	90	90
V (Å^3)	1324.3(14)	2025.89(9)	2912(2)	5069(3)	4979(3)
Z	2	4	2	4	4
F(000)	582	976	1196	2392	2400
D_{calcd} (g/cm^3)	1.40	1.550	1.323	1.521	1.557
μ (mm^{-1})	0.690	0.887	0.942	1.082	1.205
θ_{min}, θ_{max}	3.05, 27.48	2.83, 32.04	3.05, 27.48	2.96, 27.49	3.63, 27.49
ω frame width (deg)	1.1	1.9	1.3	1.1	1.0
time per frame (*s*)	60	30	60	150	30
total number of measured intensities	17 332	29 128	33 137	30 277	16 672
number of unique data	5901	7024	6553	5815	5491
observed reflections [$I > 2\sigma(I)$]	5157	5380	4911	4303	4654
number of refined variables (*n*)	284	220	281	277	277
R_1 (*F*)[a]	0.0377	0.0402	0.0527	0.0402	0.0409
[b]wR_2 (*F*)[b]	0.0971	0.1009	0.1497	0.0971	0.0671
GOF[c]	1.045	1.034	1.032	1.036	1.082
weighting parameters[d]	$a = 0.0467$	$a = 0.0472$	$a = 0.0754$	$a = 0.0480$	$a = 0.0222$
	$b = 0.2215$	$b = 0.7479$	$b = 2.4999$	$b = 4.7547$	$b = 7.4604$
largest difference map hole and peak (e Å^{-3})	−0.23	−0.411	−0.581	−0.545	−0.329
	0.23	0.334	0.572	0.471	0.368

[a] $R_1 = \sum_n||F_o| - |F_c||/\sum_n|F_o|$ for $I > 2\sigma(I)$. [b] $wR_2 = [\sum_n w(F_o^2 - F_c^2)^2/\sum_n w(F_o^2)^2]^{1/2}$ for $I > 2\sigma(I)$. [c] GOF $= [\sum_n w(F_o^2 - F_c^2)^2/(n - p)]^{1/2}$. [d] $w = 1/[\sigma^2(F_o^2) + (aP)^2 + bP]$, $P = [\max(F_o^2,0) + 2F_c^2]/3$.

and the resulting oil was extracted with CH_2Cl_2 and washed with water. The organic extract was purified by column chromatography over silica with CH_2Cl_2/PE (3:1) as the eluent to afford TTF **3b** (445 mg, 63%) as a red powder; mp 116−118 °C and $R_f = 0.79$. ^{1}H NMR ($CDCl_3$, δ): 2.43 (s, 3H), 2.44 (s, 3H), 2.45 (s, 3H), 2.48 (s, 6H), 17.24 (s, 1H). ^{13}C NMR ($CDCl_3$, δ): 18.2, 18.3, 24.0, 101.9, 109.0, 110.1, 118.7, 126.1, 126.8, 131.0, 196.6. IR (KBr, cm^{-1}): 1582 (C═O, vbr). HRMS: calcd for $C_{14}H_{16}O_2S_8$, 471.8916; found, 471.8917. Anal. Calcd for $C_{14}H_{16}O_2S_8$: C, 35.67; H, 3.18; S, 54.35. Found: C, 35.83; H, 3.36; S, 54.62.

General Procedure for the Synthesis of M(TTFSacac)$_2$(pyridine)$_2$. To a solution of TTF(acacH) (0.2 mmol) in 15 mL of THF was slowly added a methanolic solution of $M^{II}(OAc)_2 \cdot xH_2O$ (0.1 mmol) at 0 °C. The mixture was allowed to stir for 10−40 min at 0 °C. The orange precipitate was filtrated, washed with MeOH and then Et_2O, and sucked dry. The precipitate was dissolved in pyridine, and pentane was added slowly to form two phases. Crystals were harvested after a slow diffusion of the pentane into the pyridine solution.

Ni(TTFSacac)$_2$(pyridine)$_2$, 6a. 71% yield, mp 135−136 °C. IR (KBr, cm^{-1}): 1575. HRMS: calcd for $C_{40}H_{54}O_4S_{16}Ni$ [M-2pyridine]$^+$, 1167.8907; found, 1167.8908.

Ni(TTFSacac)$_2$(pyridine)$_2$, 6b. 75% yield, mp 211−216 °C. IR (KBr, cm^{-1}): 2999, 2916, 1599, 1574, 1471, 1419, 1378, 1336. HRMS: calcd for $C_{28}H_{30}O_4S_{16}Ni$ [M-2pyridine]$^+$, 999.7029; found, 999.7015. Anal. Calcd for $C_{38}H_{40}N_2O_4S_{16}Ni$: C, 39.42; H, 3.29; N, 2.42; S, 44.26. Found: C, 39.75; H, 3.41; N, 2.66; S, 44.21.

Zn(TTFSacac)$_2$(pyridine)$_2$, 7b. 61% yield, mp 152−154 °C. ^{1}H NMR ($CDCl_3$, δ): 2.39 (s, 6H, CH_3), 2.41 (s, 6H, CH_3), 2.43 (s, 6H, CH_3), 2.52 (s, 12H, CH_3), 7.45 (m, 2H, CH), 7.82 (m, 1H, CH), 8.59 (m, 2H, CH). ^{13}C NMR ($CDCl_3$, δ): 19.3, 19.4, 19.5, 29.9, 102.7, 109.1, 112.2, 114.4, 124.9, 127.0, 128.7, 138.0, 138.5, 149.7, 199.1. IR (KBr, cm^{-1}): 2578, 2385, 2262, 1985, 1962, 1599, 1579, 1443, 1374. HRMS: calcd for $C_{28}H_{30}O_4S_{16}Zn$ [M-2pyridine]$^+$, 1005.6967; found, 1005.6978.

Single-Crystal Structure Determination. A single crystal of each compound was carefully selected under a polarizing microscope and glued to a thin fiber of glass. Single-crystal data collection has been performed at RT with a Nonius KappaCCD diffractometer (Centre de Diffractométrie, Université de Rennes, France) with Mo Kα radiation ($\lambda = 0.71073$ Å). A crystal-to-detector distance of 25.0 mm has been used for all the crystals, and data-collection strategies (determination and optimization of the goniometer positions) have been performed with the help of the COLLECT program (Nonius 1998).[15] Experimental details of the data collection have been summarized in Table 1.

Finally, integration processing and data reduction have been carried out using the EVAL program.[16] Merging the procedure and additional spherical-type absorption corrections have then been applied through the SADABS program.[17a] Structure determination has been performed with the direct-methods solving program SIR97,[18] which revealed all the non-hydrogen atoms. The SHELXL program[17b] has been used to refine the structure. Finally, hydrogen atoms were placed geometrically and held in riding mode in the least-squares refinement procedure. The last cycles of the refinement included atomic positions for all the atoms, anisotropic displacement parameters for all the non-hydrogen atoms, and isotropic displacement parameters for all the hydrogen atoms. Large values of U_{eq} for the C6 and C7 atoms of one butyl chain in the structure of the **3a** compound have been taken into account through a disordered

(15) *Nonius 1998*; COLLECT, KappaCCD software; Nonius BV: Delft, The Netherlands, 1998.
(16) Duisenberg, A. J. M. Reflections on Area detectors. Thesis, Utrecht University, Utrecht, The Netherlands, 1998.
(17) (a) Sheldrick, G. M. *SADABS*, version 2.03; Bruker AXS, Inc.: Madison, WI, 2002. (b) Sheldrick, G. M. *SHELX97*; Program for the Refinement of Crystal Structures; University of Göttingen: Göttingen, Germany, 1997.
(18) Altomare, A.; Burla, M. C.; Camalli, M.; Cascarano, G.; Giacovazzo, C.; Guagliardi, A.; Moliterni, A. G. G.; Polidori, G.; Spagna, R. *J. Appl. Crystallogr.* **1999**, *32*, 115−119.

Scheme 1

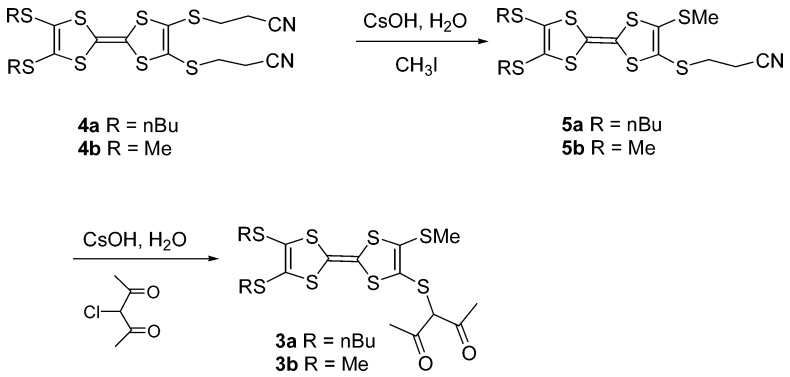

alkane chain. Such a disorder model (two pathways for the C8−C7−C6−C5 chain with identical populations) has been introduced in the least-squares refinement and lead to realistic U_{eq} values, better refinement agreement factors, and residual electronic density values. Similarly, in the case of the **6bA** crystal, the C19 atom, with a large value of U_{eq}, has been split into two atomic positions, C19A and C19B, with identical populations.

Details of the final refinements are given in Table 1 for all compounds.

Magnetic Measurements. Magnetic susceptibility measurements on **6b** (17.09 mg) and **7b** (14.28 mg) were obtained on a finely ground polycrystalline sample with the use of a Quantum Design SQUID magnetometer MPMS-XL. The direct current measurements were collected from 1.8 to 300 K and from −70 to 70 kOe. Experimental data were also corrected for the sample holder and for the diamagnetic contribution calculated from Pascal constants.[19]

Results and Discussion

The new ligands were prepared from the dissymmetrical TTFs **4a,b**,[12] according to the chemical pathway depicted in Scheme 1. Both TTF **4a** and TTF **4b** are protected precursors of TTF dithiolates which can be generated under basic conditions. One thiolate protecting group can be selectively cleaved with 1 equiv of cesium hydroxide monohydrate, and the addition of iodomethane leads to TTF **5a** and TTF **5b**,[13] respectively, in excellent yields. Deprotection of the second thiolate group, under the same conditions followed by the nucleophilic substitution with 3-chloro-2,4-pentanedione, affords TTFSacacHs **3a** and **3b** in 79 and 63% yields, respectively (Scheme 1). These two new TTFSacacHs, **3**, are purified by chromatography over a silica gel column.

Single crystals of both acetylacetone substituted TTF **3a** and acetylacetone substituted TTF **3b** were obtained. For **3a**, they were harvested from a mixture of dimethylsulfoxide (DMSO) and chloroform (1:1) while a slow diffusion of MeOH in a dichloromethane solution of TTF **3b** allowed us to isolate dark red crystals. The Oak Ridge thermal ellipsoid plot (ORTEP) diagrams of **3a** and **3b** are given in Figures 1 and 2, respectively. Both TTFs present similar trends such as a TTF core almost planar and the acetylacetone substituent located in a plane almost perpendicular to the plane formed by the TTF core with angles of about 100 and 104° for **3a** and **3b**, respectively. The bond lengths within the acetylacetone group (acacH) in both structures are quite different. For **3a**, the carbonyl bond lengths, C(17)−O(2) and C(19)−O(1), are of comparable value [1.299(5) and 1.284(4) Å, respectively], whereas for **3b** these bond lengths, C(11)−O(2) and C(13)−O(1), are different [1.264(3) and 1.302(3) Å, respectively]. Similar observations can be performed on the C−C bond lengths for **3a**; the C(17)−C(18) and C(18)−C(19) bond lengths are similar [1.410(5) and 1.406(5) Å, respectively], while the bond length values for **3b** C(13)−C(10) and C(10)−C(11) are different [1.394(3) and 1.430-(3) Å, respectively]. Both sets of data are consistent with

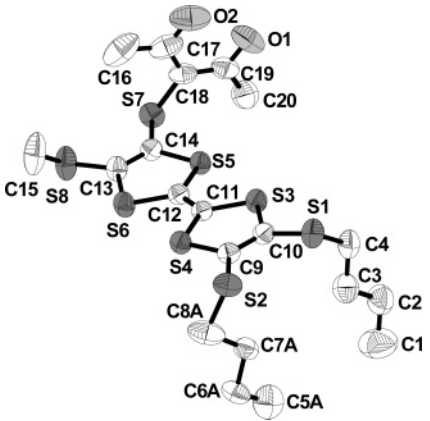

Figure 1. ORTEP view of TTFSacacH **3a** showing the atom labeling (50% probability ellipsoids). Hydrogen atoms are omitted and only one position of the disordered butyl chain is shown for clarity. Selected bond lengths in Å: C11−C12, 1.345(3); C14−S7, 1.754(3); S7−C18, 1.772(3); C17−O2, 1.299(5); C19−O1, 1.284(4); C17−C18, 1.410(5); and C18−C19, 1.406-(5).

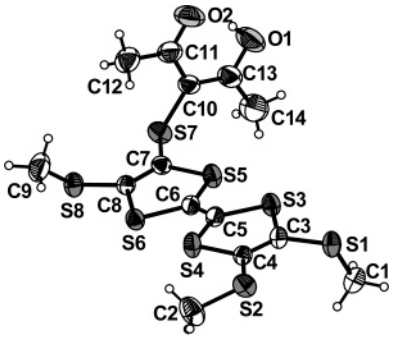

Figure 2. ORTEP view of TTFSacacH **3b** showing the atom labeling (50% probability ellipsoids). Selected bond lengths in Å: C6−C5, 1.345-(2); C7−S7, 1.7540(16); S7−C10, 1.7713(19); C11−O2, 1.264(3); C13−O1, 1.302(3); C13−C10, 1.394(3); and C10−C11, 1.430(3).

(19) Boudreaux, E. A., Mulay, L. N., Eds. *Theory and Applications of Molecular Paramagnetism*; John Wiley & Sons: New York, 1976.

Scheme 2

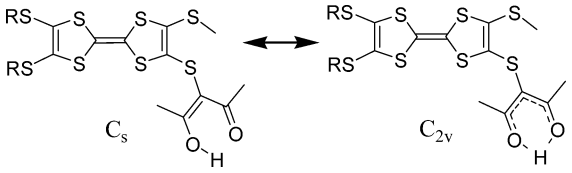

the fact that these TTFs are present in the solid state in the enol form. The data also suggest that, in TTF **3a**, the H atom is shared symmetrically with the O atoms with a complete π-delocalization; this H atom could not be identified in the last Fourier difference map. In the case of TTF **3b**, an asymmetric structure is obtained with the H atom localized on O1 (Figure 2).

Actually, these data are consistent with previous observations for β-diketones such as acetylacetone derivatives, where two enolic forms can be envisioned as depicted in Scheme 2:[20] a symmetric (C_{2v}) structure where the C—O and C═O as well as the C—C and C═C bond distances become equal to each other and the H atom lies midway between the two oxygens (O—H—O), such as in TTF **3a**, and an asymmetric (C_s) structure where the C—O and C═O as well as the C—C and C═C are different, as observed for **3b**. Moreover, the shorter O···O distance in **3a**, being equal to 2.421 Å, when compared with the O···O distance in **3b** (2.451 Å), is in favor of a C_{2v} symmetry.

Interestingly, organization of these two TTF(SacacH)s in the solid state is different. TTFs **3a** form stacks (Figure 3) with a segregation between the lipophilic parts of the ligands (thiobutyl chains) and the hydrophilic parts (acetylacetone substituents). A large longitudinal slip is observed between two neighboring TTFs, with the shortest S···S contacts being equal to 3.752 (S5···S3) and 3.759 Å (S6···S4).

Contrariwise, analysis of the organization of TTF **3b** in the solid state reveals a segregation of the acetylacetone moieties along the *a* axis (Figure 4) with the acetylacetone substituent of one TTF facing the sulfur atom of the dithiole ring of another TTF with a head-to-tail organization of these two TTFs, as represented in Figure 4.

Ni and Zn Complexes. Coordination of TTF **3a** and TTF **3b** has been achieved by a reaction at 0 °C of a methanolic solution of $M^{II}(OAc)_2 \cdot H_2O$ (M = Ni^{2+}, Zn^{2+}) with a concentrated THF solution of the TTF ligand. The addition of methanol induces the formation of an orange precipitate that evolves quantitatively upon attempted chromatography on silica gel into the starting ligand. The analysis by high-resolution mass spectrometry (HRMS) of the precipitate confirmed the formation of the metal-linked TTF dimers, $M(TTFSacac)_2$. Crystals of the Ni and Zn complexes starting from TTF **3b** were successfully grown by slow diffusion of pentane into a concentrated pyridine solution of the precipitate (Scheme 3). The crystal structure analysis reveals that **6b** and **7b** are mononuclear complexes with two coordinated $(MeS)_3$TTFthioacetylacetonates, TTFSacac, and solvated by two pyridines to give hexacoordinated metal centers,

(20) Srinivasan, R.; Feenstra, J. S.; Park, S. T.; Xu, S.; Zewail, A. H. *J. Am. Chem. Soc.* **2004**, *126*, 2266 (and references therein).

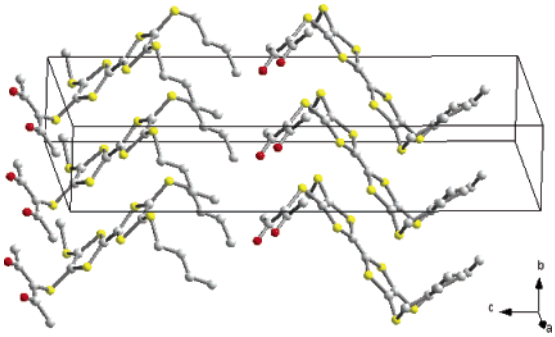

Figure 3. View of the unit cell of TTF **3a** projection showing a herringbone-like arrangement of the TTF stacks.

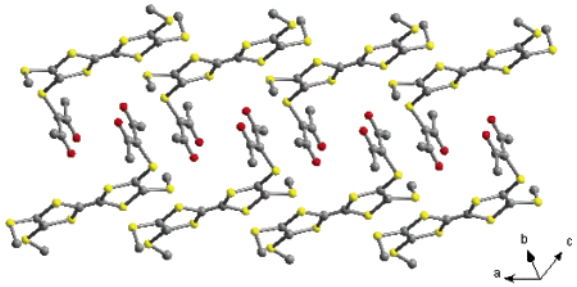

Figure 4. Stacking of the acetylacetone moieties along the *a* axis in TTFacacH, **3b**.

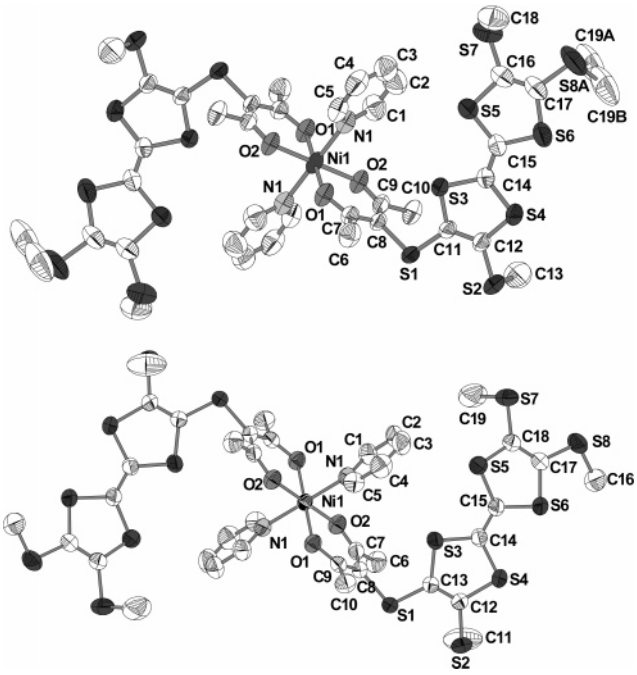

Figure 5. ORTEP drawing of the two concomitant polymorphs Ni(TTFSacac)$_2$(pyridine)$_2$ **6bA** (top) and **6bB** (bottom). H atoms are omitted for clarity, and ellipsoids are drawn at 50% probability.

$M(TTFSacac)_2(pyridine)_2$ **6b** (M = Ni^{II}) and **7b** (M = Zn^{II}). In the case of the nickel complex, $Ni(TTFSacac)_2(pyridine)_2$, two types of crystals have been obtained in the same batch of crystallization: orange needles (crystal **A**) and orange prisms (crystal **B**). Structural determination of the crystalline Zn^{II} complex **7b**, $Zn(TTFacac)_2(pyridine)_2$, showed that it is isostructural to the orange prisms of the Ni^{II} complex **6b** (crystal B). The X-ray molecular structures of **6bA**, **6bB**, and **7b** are shown in Figures 5 and 6, and selected bond

Scheme 3

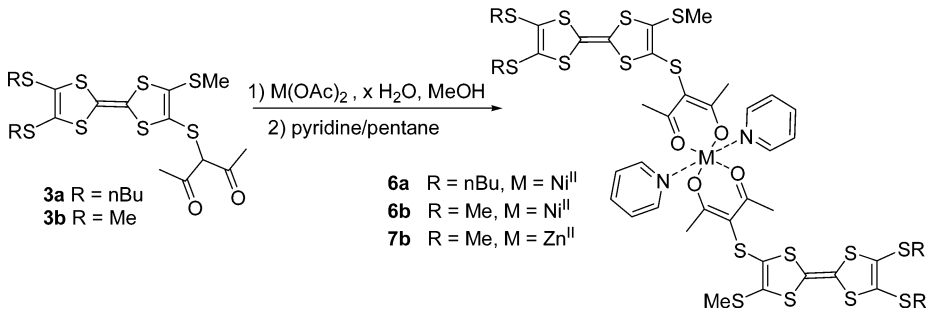

Table 2. Selected Bond Distances (Å) for **6bA**, **6bB**, and **7b**

6bA Ni(TTFacac)$_2$(pyridine)$_2$ crystal A		**6bB** Ni(TTFacac)$_2$(pyridine)$_2$ crystal B		**7b** Zn(TTFacac)$_2$(pyridine)$_2$	
Ni1−O2	2.009(2)	Ni1−O1	2.0125(17)	Zn1−O1	2.0453(14)
Ni1−O1	2.010(2)	Ni1−O2	2.0139(16)	Zn1−O2	2.0494(13)
Ni1−N1	2.126(3)	Ni1−N1	2.131(2)	Zn1−N1	2.207(2)
S1−C11	1.753(3)	S1−C13	1.750(2)	S1−C13	1.751(2)
S1−C8	1.774(3)	S1−C8	1.766(2)	S1−C8	1.7675(19)
S3−C11	1.748(3)	S3−C13	1.759(3)	S3−C13	1.758(2)
S3−C14	1.761(3)	S3−C14	1.762(2)	S3−C14	1.7654(19)
S4−C14	1.746(3)	S4−C14	1.757(3)	S4−C14	1.759(2)
S4−C12	1.757(3)	S4−C12	1.758(3)	S4−C12	1.765(2)
S5−C15	1.755(4)	S5−C15	1.749(3)	S5−C15	1.752(2)
S5−C16	1.756(4)	S5−C18	1.763(3)	S5−C18	1.771(2)
S6−C15	1.752(3)	S6−C15	1.754(2)	S6−C15	1.7599(19)
S6−C17	1.759(5)	S6−C17	1.756(3)	S6−C17	1.762(2)
O1−C7	1.253(4)	O1−C9	1.258(3)	O1−C9	1.263(2)
O2−C9	1.252(4)	O2−C7	1.253(3)	O2−C7	1.257(2)
C7−C8	1.422(5)	C7−C8	1.425(4)	C7−C8	1.427(3)
C8−C9	1.416(5)	C8−C9	1.421(3)	C8−C9.	1.423(3)
C14−C15	1.339(5)	C14−C15	1.339(3)	C14−C15	1.341(3)

lengths and angles are listed in Table 2. In all structures, the molecules appear as trans isomers with the metal(II) center chelated by two TTFacac units in the equatorial plane and with each TTF core pointing in opposite directions from the plane of the molecule. The octahedral coordination geometry around the metal is completed by two axial pyridine ligands, as shown in Figures 5 and 6. The central C═C bond lengths of the TTF cores [1.339(5) Å in **6bA**, 1.339(3) Å in **6bB**, and 1.341(3) Å in **7b**] are in the average range for neutral donor cores within these complexes. Where the [Ni(TTFSacac)$_2$(pyridine)$_2$] complexes **6b** are concerned, analysis of the bond lengths in these two concomitant polymorphs does not reveal drastic differences between **A** and **B** on the TTF cores or on the metallic Ni(acac)$_2$ bridge. The Ni−O distances are within 2.009(2)−2.0139(16) Å and are shorter than the Ni−N one, 2.126(3)−2.131(2) Å, as a result of the negative charge and the chelating coordination mode of the acetylacetonate ion part. Similar observations can be realized on the Zn(TTFSacac)$_2$(pyridine)$_2$ complex **7b**.

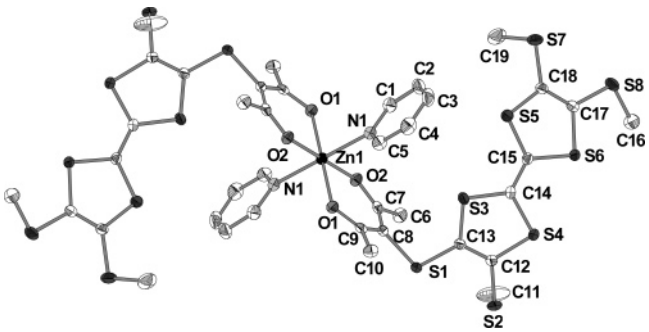

Figure 6. ORTEP drawing of the Zn(TTFSacac)$_2$(pyridine)$_2$ complex **7b**. H atoms are omitted for clarity, and ellipsoids are drawn at 50% probability.

The main differences between the two Ni polymorphs lie in the conformation of the donor core, the Ni(acac)$_2$ motif, and their relative orientation. Where the TTF itself is concerned, the donor core is not planar, with a folding of each dithiole ring more or less pronounced along the S···S axis. The values of the torsion angles along the S···S vector reach 13 and 19° in **6bA**, while they amount to 18 and 19° in **6bB**. The chelate ring around the metal in **6bA** is essentially planar, while in **6bB**, the six-membered metallacycle is slightly distorted. The packing motifs of the molecules **6bA** and **6bB** are also different. Indeed, for **6bA**, a large cavity (233 Å^3/unit cell, 8%) can be observed along the *a* axis, leading to the formation of channels where no residual electronic density could be found in the Fourier difference map (Figure 7), while for **6bA**, the packing is more compact. This induces large differences in the density of the crystals, as it amounts to 1.323 and 1.521 g/cm^3 for **6bA** and **6bB**, respectively.

Magnetic Properties. As expected for the Zn complex, the magnetic susceptibility is diamagnetic around -7×10^{-4} cm^3/mol. On the other hand, the compound **6b** is paramagnetic, following a Curie law down to 50 K ($C = 1.06$ cm^3 K/mol, see the χT vs T plot in Figure 8, with the data measured at 1000 Oe). The Curie constant is close to the

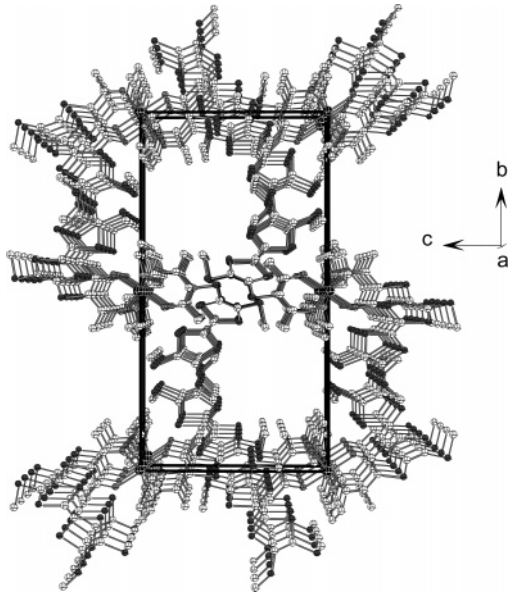

Figure 7. Projection view along the *a* axis showing the empty channels of the polymorph Ni(TTFSacac)$_2$(pyridine)$_2$, **6bA**.

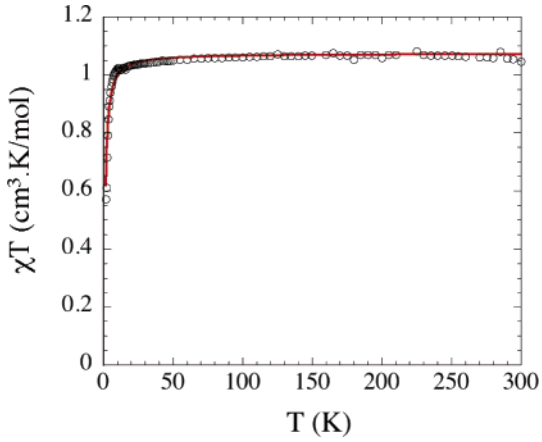

Figure 8. Temperature dependence of the χT product for the $S = 1$ Ni complex, **6b**. The solid line is the best fit obtained using the model described in the text.

expected value of 1 cm^3 K/mol for an isolated $S = 1$ Ni^{II} with $g = 2$. For this monomer, the decrease of the χT product at low temperature is without doubt the signature of the zero-field splitting effect, which is well-known for Ni(II).[21] The magnetic behavior of **6b** was, thus, modeled considering the following Hamiltonian, $H = DS_z^2 + g\mu_B SH$, and the best set of parameters obtained is $g = 2.07$ and $D/k_B = +2.1$ K (Figure 8).[22]

Redox Behavior. The redox behavior of these new complexes was investigated by cyclic voltammetry. The experiments were carried out on M(TTFSacac)$_2$(pyridine)$_2$ crystals, **6b** (M = Ni) and **7b** (M = Zn). As can be seen in Figure 9, all the complexes exhibit two main reversible systems, the first one being broader (+0.00 V for **6b** and +0.00/+0.08 V for **7b** vs Fc$^+$/Fc) than the second one (+0.33 V for **6b** and +0.37 V for **7b** vs Fc$^+$/Fc). Thin-layer cyclic voltammetry showed that each system involves the

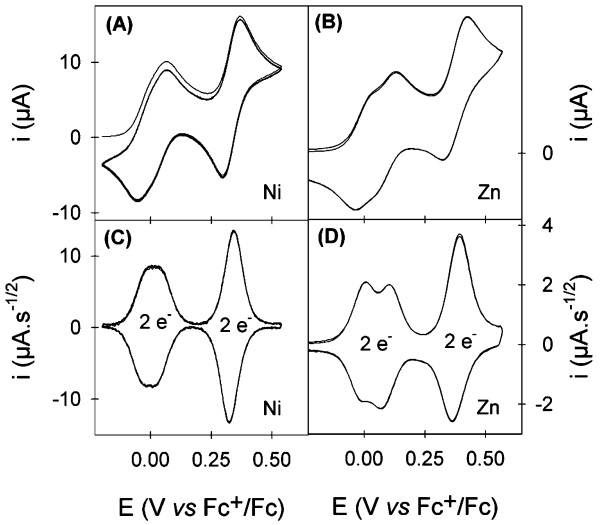

Figure 9. Cyclic voltammogram (A and B) and deconvoluted cyclic voltammogram (C and D) of **6b** and **7b** (2.5×10^{-4} M) in 0.2 M TBAHP/CH_2Cl_2.

exchange of two electrons. Actually, the first oxidation wave was deconvoluted into two peaks corresponding to a one-electron process for each with a well-defined separation for the Zn derivative **7b**. On the other hand, the second oxidation wave is a two-electron process.

The splitting of the first system indicates that the two TTF cores in one complex oxidize successively into cation radical species, and then both TTF cation radicals oxidize simultaneously into the dication species, accordingly to the sequence described in Scheme 4. This splitting, being independent of the concentration (between 10^{-6} and 8×10^{-4} M), shows that the existence of intramolecular electronic interactions is clearly demonstrated. This behavior is reminiscent of what was previously observed on dimeric TTFs where intramolecular interactions between the two donor moieties, either through space or through a bond, were electrochemically evidenced.[23] These interactions are extremely variable depending on the type of connection used, where the connections are made, and how many connections are placed between the two TTFs. The through-bond interactions are generally weak; for instance, for dimeric TTFs linked by an ethylene[24] or acetylene[24] spacer (Scheme 5), no splitting of the two redox systems is observed. Contrariwise, for more rigid molecules such as benzo-,[25] pyrazine-,[26] and dihydrophosphinine-fused[27] bisTTFs, splitting of the two redox processes into four one-electron reversible oxidations occurs. When the through-space interactions within bisTTFs are now considered, close proximity of the redox cores is at the origin of the splitting of the oxidation steps. For example, most of the bisTTFs that are linked by a single linkage and exhibiting a splitting of the first redox process possess a short, nonconjugated spacer group such as a methylenedithio or

(21) Carlin, R. L. *Magnetochemistry*; Springer-Verlag: New York, 1986.
(22) O'Connor, C. J. *Prog. Inorg. Chem.* **1982**, *29*, 203.
(23) Iyoda, M.; Hasegawa, M.; Miyake, Y. *Chem. Rev.* **2004**, *104*, 5085.
(24) Otsubo, T.; Kochi, Y.; Bitoh, A.; Ogura, F. *Chem. Lett.* **1994**, 2047.
(25) Adam, K.; Müllen, K. *Adv. Mater.* **1994**, *6*, 439.
(26) Lahlil, K.; Moradpour, A.; Merienne, C.; Bowlas, C. *J. Org. Chem.* **1994**, *59*, 8030.
(27) Avarvari, N.; Fourmigué, M. *Chem. Commun.* **2004**, 2794.

Scheme 4

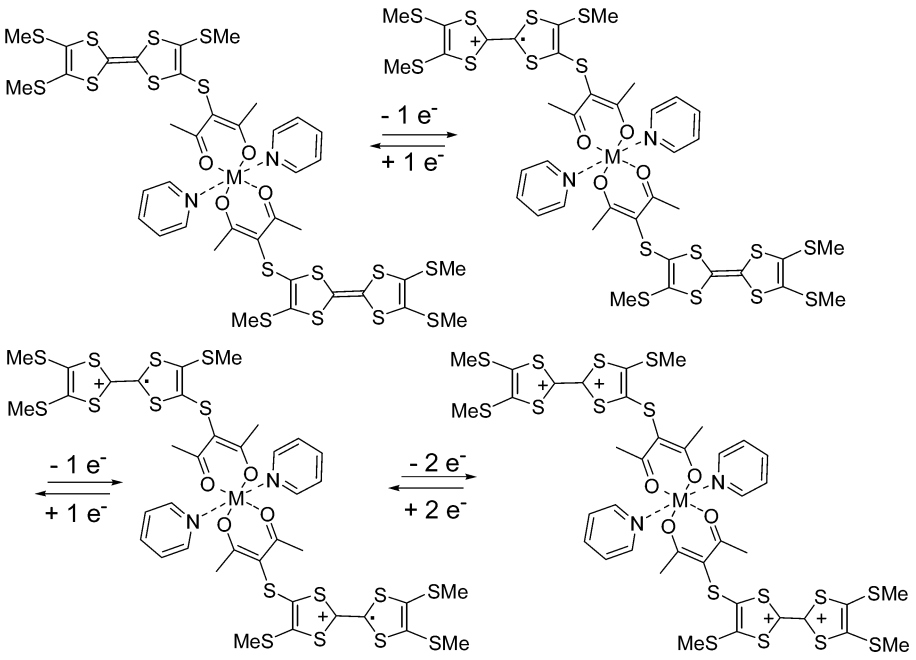

Scheme 5

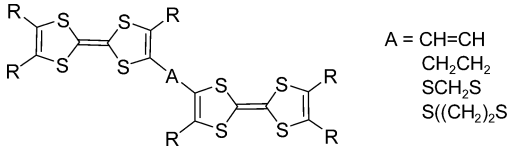

an ethylenedithio linker (Scheme 5).[23,28−30] To explain the multiredox stages of such bisTTFs, a sandwich structure was postulated that contributes to the stabilization of the mono-radical cation species through overlap interactions. As a result of Coulombic repulsion, removal of the second electron induces the opening out of the molecule followed by the concomitant withdrawing of the latest two electrons from the now two non-interactive redox centers. A longer spacer group, for example, a one-propylene dithio bridge, between the two TTF cores induces the disappearance of the splitting of the first oxidation system.[28] Interestingly, to the best of our knowledge, among the few metallic complexes involving two TTF cores, no interaction has been evidenced electrochemically between the donor cores.[2−7] Therefore, taking into account the literature where it can be seen that close proximity of the redox core is generally at the origin of the three redox reversible systems, it is unlikely that the splitting observed for **6b** and **7b** is simply due to intramolecular Coulombic effects between the TTFs. Actually, in accordance with the molecular structure, the distance between the two exocyclic sulfurs (S1) connecting the TTF moieties to the metal(acac)$_2$ amounts to 10.21 Å within **6b** and 10.25 Å for **7b**. Even with a different conformation than the one observed in the solid state, the TTFs are too far apart to interact through space. Therefore, the splitting observed here could be tentatively attributed to interactions through bonds which involve the metal(acac)$_2$ bridge.

These interactions between the two TTF cores within **6b** and **7b** are also confirmed by the UV−visible−near infrared (UV−vis−NIR) investigation carried out after the chemical oxidation of M(TTFSacac)$_2$(pyridine)$_2$ by a successive aliquot addition of $NOSbF_6$ (Figure 10). In both cases, chemical oxidation with 1 equiv of $NOSbF_6$ leads to the appearance of new bands that are characteristic to the formation of the cation radical species (460 and 880 nm for **6b** and 450 and 870 nm for **7b**). As expected, the maximum absorption for the two former bands is obtained with 2 equiv of the oxidizing agent. Interestingly, a weaker and broader band is also observed at 2200 nm, which reaches its maximum with 1 equiv of the oxidizing agent and disappears upon the addition of another equivalent of $NOSbF_6$. This band, more intense for **7b** than for **6b,** is independent of the concentration in CH_2Cl_2, and it is observed at low concentration ($<10^{-4}$ M) in a mixture of CH_3CN/CH_2Cl_2. These characteristics suggest the formation of an intramolecular mixed-valence species during the addition of 1 equiv of $NOSbF_6$.

UV−vis−NIR spectroelectrochemical experiments were also performed with **6b** and **7b** despite the low solubility of these compounds in a solution with a supporting electrolyte (TBAHP/CH_2Cl_2). The bands, characteristic of radical cation species, were confirmed, and those of dication species were observed at 720 nm only for **6b** (Figure 11). An adsorption phenomenon, occurring during the second oxidation step of **7b**, did not allow the observation of the bisdication **7b**$^{4+}$. In the NIR range between −0.1 and 0.1 V versus Fc^+/Fc, the broad band at 2200 nm with a maximum at 0.0 V was observed only for **7b**. For **6b**, the close proximity of the two oxidation processes and the low solubility of **6b** in the medium do not support the observation of a NIR band by spectroelectrochemistry. In agreement with the results ob-

(28) Jørgensen, M.; Lestrup, K. A.; Bechgaard, K. *J. Org. Chem.* **1991**, *56*, 5684.
(29) Bryce, M. R.; Marshallsay, G. J.; Moore, A. J. *J. Org. Chem.* **1992**, *57*, 4859.
(30) Sudmale, I. V.; Tormos, G. V.; Khodorkovsky, V. Y.; Edzina, A. S.; Neilands, O. J.; Cava, M. P. *J. Org. Chem.* **1993**, *58*, 1355.

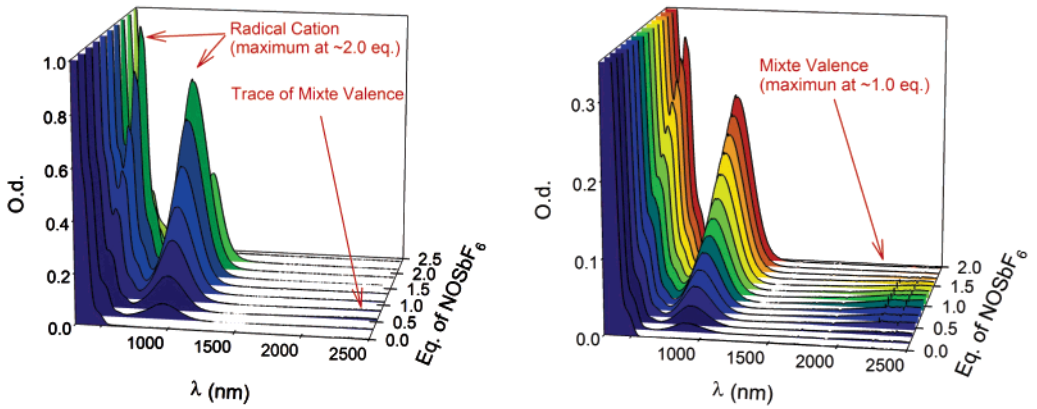

Figure 10. UV−vis−NIR spectra of **6b** (left) and **7b** (right; 8×10^{-3} M) and its corresponding oxidized species during a successive addition of $NOSbF_6$ in CH_2Cl_2.

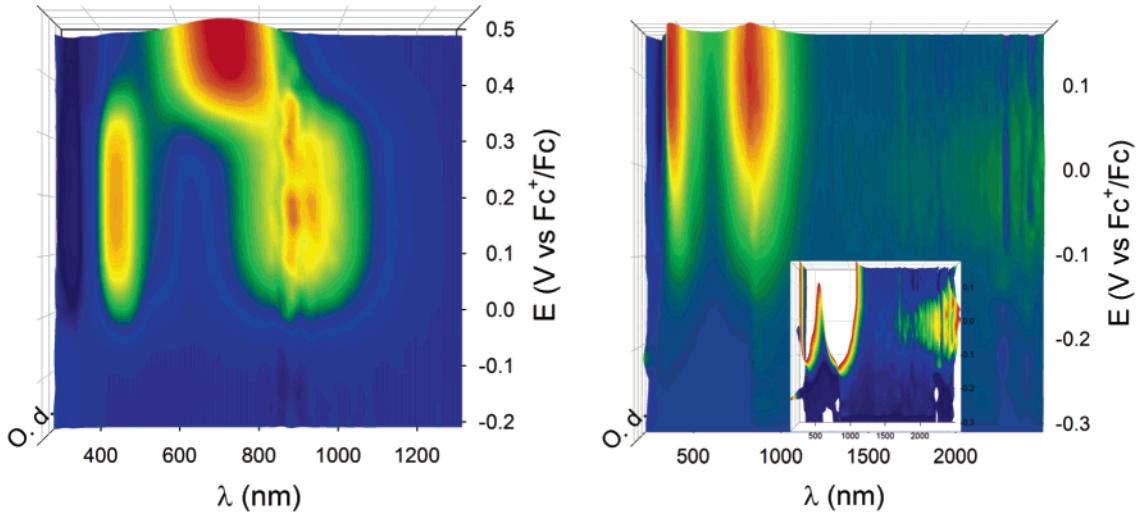

Figure 11. Difference UV−vis−NIR spectroelectrogram of **6b** (left) and **7b** (right) (2.5×10^{-4} M) in 0.2 M TBAHP/CH_2Cl_2. The first spectrum recorded at the starting potential (−0.2 V) was systematically subtracted from all the others. All the resulting "difference spectra" were then assembled in a three-dimensional plot (variation of absorbance/applied potential/wavelength) called a "difference spectroelectrogram".

tained by chemical oxidation, the NIR band of **7b** is assigned to the formation of a mixed-valence species. Moreover, the fact that this band was observed in a highly polarizing medium used for electrochemistry and by chemical oxidation confirms the formation of an intramolecular mixed-valence species.

Conclusions

The synthesis and the chelating ability of the tetrathiafulvenyl−acetylacetonate anion have been investigated in regard to metal M^{II} cations (M^{II} = Ni, Zn) giving rise to the first metal complexes involving such redox-active ligands. Electrochemical and spectroscopic investigations have evidenced intramolecular interactions between the two TTF cores of a complex, an original feature among the few metallic complexes involving two TTF cores described so far. An increased stability of the mixed-valence species is observed through the simple change of the metal cation from Ni to Zn. Further investigations on this novel attractive system will be devoted to the study of other metal cations to determine their influence on the mixed-valence species stabilization, a prerequisite for the elaboration of conducting materials by electrocrystallization.

Supporting Information Available: X-ray crystallographic files in CIF format for complexes **3a**, **3b**, **6bA, 6bB**, and **7b**. This material is available free of charge via the Internet at http://pubs.acs.org.

IC051017R